AGU ADVANCING EARTH AND SPACE SCIENCE

Geophysical Research Letters

RESEARCH LETTER
10.1029/2020GL091576

Key Points:

- New map of effective elastic thickness (T_e) for Antarctica
- Known and suspected cratonic areas have high T_e
- A low-T_e corridor meanders between these, joining the Lambert Rift, Gamburtsev Subglacial Mountains, and Dronning Maud Land passive margin escarpment

Supporting Information:

- Supporting Information S1

Correspondence to:
C. Swain,
c_swain@wt.com.au

Citation:
Swain, C. J., & Kirby, J. F. (2021). Effective elastic thickness map reveals subglacial structure of East Antarctica. *Geophysical Research Letters*, *48*, e2020GL091576. https://doi.org/10.1029/2020GL091576

Received 20 NOV 2020
Accepted 22 DEC 2020

Effective Elastic Thickness Map Reveals Subglacial Structure of East Antarctica

C. J. Swain[1] and J. F. Kirby[1]

[1]School of Earth and Planetary Sciences, Curtin University, Perth, WA, Australia

Abstract East Antarctica is the least well-exposed Precambrian shield on Earth. What is known, or surmised, of its geological structure comes from extrapolation over large distances and from geophysics. Here, we present a map of effective elastic thickness, T_e, computed from Antarctic bedrock topography and both terrestrial and satellite gravity data. T_e is directly related to lithospheric strength and can distinguish domains of differing tectonic history. Our map reveals a broad region of high T_e in Wilkes Land, interpreted as a craton, while elsewhere a corridor of low T_e meanders between areas of higher T_e. The low-T_e belt follows the trend of prominent linear magnetic anomalies identified in the Gamburtsev and Dronning Maud Land provinces, two of which have previously been identified as possible Grenville or Pan-African age sutures.

Plain Language Summary This paper presents a new, high-resolution map of the effective elastic thickness of the lithosphere of Antarctica. It is interpreted as indicating the tectonic structure of East Antarctica in the form of cratons and orogenic belts.

1. Introduction

Antarctica contains almost 10% of Earth's continental crust, but ice conceals its age, composition, and structure. Sparse coastal outcrop (Boger, 2011; Fitzsimons, 2003; Harley et al., 2013) and transported detritus (Veevers & Saeed, 2011, 2013) suggest that the East Antarctic interior comprises Archaean and Palaeoproterozoic cratons juxtaposed along Ediacaran to Cambrian age orogenic belts. This was long thought to conflict with seismic evidence for uniformly thick lithosphere (An et al., 2015a; Ritzwoller et al., 2001) suggestive of a single craton, but recent higher-resolution results (Shen et al., 2018) show significant variations in the uppermost mantle lithosphere. Poor knowledge of subglacial geology also limits interpretation of East Antarctic topography, including the enigmatic Gamburtsev Sub-glacial Mountains (GSM) in the center of the continent (Ferraccioli et al., 2011).

Antarctic bedrock (Figure 1) has been largely concealed since the growth of continent-scale ice sheets about 34 million years (Myr) ago (Zachos et al., 2001). Most outcrop occurs in the Transantarctic Mountains, which are located at the boundary between the East Antarctic Shield and the Paleozoic to Mesozoic terranes of West Antarctica (Boger, 2011; Harley et al., 2013). The shield is particularly poorly exposed, but scattered outcrops at its margins are predominantly igneous and metamorphic rocks with ages between 3,800 and 480 Myr (Boger, 2011; Harley et al., 2013), which correlate closely with those parts of Australia, India and Africa that were contiguous with East Antarctica before Gondwana break-up began 180 Myr ago.

Three separate Grenville-age orogens are recognized in East Antarctica (Figure 1): the Maud, Rayner, and Wilkes Provinces (Fitzsimons, 2000). These have been correlated with pre-drift adjacent orogens in, respectively, Africa (Namaqua-Natal), India (Eastern Ghats), and Australia (Albany-Fraser), although more recent work, for example, Jacobs et al. (2020), Morrissey et al. (2015), and Wang et al. (2020) have revealed significant age differences, as well as their much larger sub-ice extents. They are separated by regions of Pan-African-age tectonism.

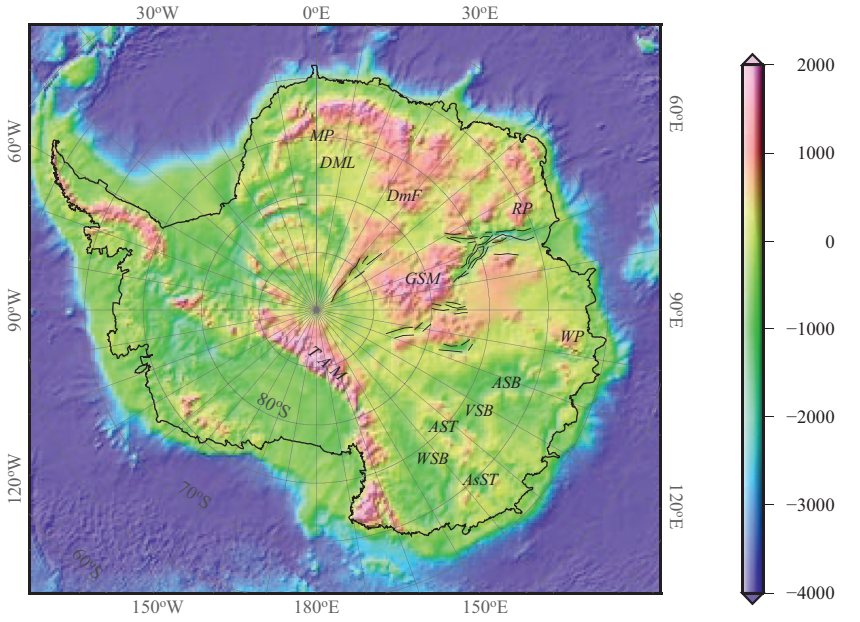

Figure 1. Bedrock elevation (m) from "BedMachine" (Morlighem et al., 2020), showing Provinces, Basins, and Trenches. ASB, Aurora Subglacial Basin; AsST, Astrolabe Subglacial Trench; AST, Adventure Subglacial Trench; DmF, Dome F; DML, Dronning Maud Land; GSM, Gamburtsev Subglacial Mountains; MP, Maud Province; RP, Rayner Province; TAM, Transantarctic Mountains; WP, Wilkes Province; WSB, Wilkes Subglacial Basin; VSB, Vincennes Subglacial Basin (Cianfarra & Maggi, 2017; Cianfarra & Salvini, 2016). East Antarctic Rift System shown as short black lines. (The spike anomaly in the top-right corner was removed prior to applying the FFT to avoid leakage into the other corners.).

2. Physiography and Geophysics

Numerous ice cores have been collected from the East Antarctic interior, but drilling has yet to intersect basement rock leaving geophysical data as the only direct constraint on subglacial topography and geology. A patchwork of regional aero geophysical surveys have identified magnetic and gravity anomalies consistent with geological evidence for cratons and orogenic belts, although, their interpretation is hindered by variable resolution and data gaps, and by the lack of outcrop to ground-truth the age of geophysical domains and lineaments.

Since about 2000, technology has been sufficiently advanced to equip a small aircraft with a magnetometer, gravity meter, and ice-thickness radar and these have been routinely used for most such surveys over Antarctica. They usually involve a uniform line spacing of between 5 km (e.g., Ferraccioli et al., 2011) and 20 km (e.g., Riedel et al., 2013) depending on the expected source depth. Line spacing is most critical for magnetic surveys since these usually have the best resolution and can convincingly map lineaments. The survey data reported by Aitken et al. (2014) used a radial line distribution with lines ~1,000 km long flown from a single base airstrip. This is a very efficient way to cover a large area, but means that line separation at their far ends is over 100 km making it hard to map magnetic lineaments, though airborne gravity, being much lower resolution, may be adequately mapped.

There have been several recent continent-wide compilations of gravity (Scheinert et al., 2016), magnetic ("ADMAP2", A. V. Golynsky et al., 2018), and ice thickness/bedrock elevations ("Bedmap2", Fretwell, 2013). A more recent bedrock compilation is "BedMachine" (Morlighem et al., 2020).

The bedrock elevation map (Figure 1) reveals that between ~100°E and 150°E (Australo-Antarctica) the bedrock of East Antarctica lies mainly below sea level, but is above sea level between 20°W and 100°E (except in parts of the East Antarctic Rift system). O'Donnell and Nyblade (2014) used this dichotomy, as well as estimates of crustal thickness, to argue that East Antarctica is not in isostatic equilibrium, possibly due to dynamic topography.

Variations in topographic relief can be shown by a map of its variance. Figure S1 shows the variance of the rock-equivalent topography (RET), which is similar to that of the bedrock elevation, and shows it to be uniformly high over East Antarctica. In particular, the bedrock elevations of the low-lying part are anomalously variable for a stable craton. Within the two major basins, the Aurora and Wilkes, lie a number of sub-basins and trenches (Figure 1) reaching to >2 km below sea level. According to Paxman et al. (2019a), these were formed by glacial erosion along pre-existing grabens within these basins. Cianfarra and Salvini (2016) and Cianfarra and Maggi (2017) proposed that these trenches are the result of Cenozoic intraplate strike-slip faulting on reactivated basement faults. Additionally, the much wider Wilkes and Aurora basins are inferred to be older tectonic features, likely Permian in age, that may reflect Pangea-wide extension that also affected interior East Antarctica (Maritati et al., 2020).

Several Moho depth studies have been carried out over Antarctica using both seismic and gravity data. An et al. (2015b) constructed a three-dimensional S-velocity model of the Antarctic lithosphere using 10,000 fundamental-mode Rayleigh wave dispersion curves from earthquake waveforms and ambient noise. They then used an empirical equation to select the Moho depths from this three-dimensional model. Pappa et al. (2019a) in a recent study compares Moho depths from seismic and gravity data, finding that these can disagree by > 10 km, notably over parts of the Gamburtsev Province. One way to reconcile these differences is to introduce an anomalously high-density lower crust beneath the northern and central Gamburtsev Province (see Supplementary Figures 5 and 6 in Ferraccioli et al., 2011).

An et al. (2015b) drew attention to the bedrock mountains of East Antarctica lying between 20°W and 100°E (Figure 1), and their crustal roots, which reach depths of 50–60 km. These mountains occur parallel to the coast in Dronning Maud Land, where they are locally exposed above the ice sheet, but also extend inland to form a subglacial range below Dome F (Figure 1) and the similar, though better known, Gamburtsev Subglacial Mountains, both of which are known only from geophysical data. Their high elevation, deep crustal roots, and alpine topography are typical of relatively young mountain belts (Creyts et al., 2014; Rose et al., 2013) which is problematic given that they occur within a shield that has no significant magmatism or metamorphism younger than 480 Myr, and in the case of the Gamburtsevs they are located in the center of a continent far removed from any modern plate boundary. Several hypotheses have been proposed to account for their formation, including two that still stand in the light of modern data.

(1) Very slow erosion of a 500 Myr-old orogen (An et al., 2015b; Fitzsimons, 2003). Several authors have studied detrital zircons from Pridz Bay, of probable Gamburtsev provenance (van de Flierdt et al., 2007, 2008; Veevers & Saeed, 2008). The zircon ages cluster in two groups: 550–500 Ma (Pan-African and most numerous) and 1,050–1,850 Ma (Grenville). Evidence for extremely low erosion rates is presented by Cox et al. (2010) and Thomson et al. (2013). A recent seismic model (Shen et al., 2018) shows a slow shear velocity anomaly in the uppermost 50 km of the mantle beneath the Gamburtsevs which earlier models had evidently lacked the resolution to detect. Shen et al. (2018) suggest that this is compositional in origin rather than thermal, possibly following a continental collision, which might support the idea that the mountains were formed in a Pan-African orogenic belt.
(2) Ferraccioli et al. (2011) proposed that the crustal root of the ancestral mountains formed in a Proterozoic (~1,000 Ma) collision possibly with the Ruker Craton. The mountains were eroded but their roots avoided delamination as their buoyancy reduced over time (Fisher, 2002). Rift-flanks were uplifted and buoyancy restored during the Permian and Cretaceous development of the East Antarctic Rift System (Figure 1); valley incision and peak uplift resulted from the cooling climate and dynamic ice sheet (34–14 Ma).

It is difficult to reconcile the available geological and geophysical data with a single model of the lithospheric architecture. Resolving these issues requires a means of mapping some quantity that is more closely related to the age and tectonic setting of the subglacial features revealed by geophysical surveys. Effective elastic thickness (T_e) should be particularly useful here as it is generally high over ancient cratons and lower over the younger orogenic belts between them (Audet & Burgmann, 2011), with heat flow and lithospheric composition being important controls on T_e (Lowry & Smith, 1995). Two other factors that weaken the lithosphere, and are both associated with mountain belts, are plate-bending stress and crust-mantle decoupling that occurs with the thickened crust of those mountains (Burov & Diament, 1995).

3. T_e Estimation

Here we employ a wavelet version of Forsyth's (1985) Bouguer coherence method to map T_e using wavelets with high spatial resolution (Kirby & Swain, 2011). The essence of Forsyth's method is to estimate the initial surface and subsurface loads using load deconvolution equations (J. F. Kirby, 2014) and use these to model the observed coherence between Bouguer gravity and topography and hence estimate T_e. The original method is applied in the wavenumber domain via the FFT, and yields estimates of the subsurface load, or the ratio between subsurface and surface load, f, as well as T_e. The wavelet method applies the same equations to estimate T_e (and possibly the load) at each point of a grid. However, as Tassara et al. (2007) point out there is often a strong anti-correlation between T_e and f, so this method of load recovery must be treated with caution if such anti-correlation is observed.

In the presence of significant erosion, the coherence method can lead to overestimations of T_e (Kirby & Swain, 2009; McKenzie, 2003). The method depends on estimating the wavelength of the transition from high to low Bouguer coherence, and erosion can effectively move this transition to longer wavelengths by destroying the coherence at the true transition wavelengths. It appears (Creyts et al., 2014) that the landscapes beneath the Gamburtsev (and probably other) Subglacial Mountains are exceptionally well preserved, and thus there is very high coherence between free air gravity and bedrock topography in the Gamburtsevs (e.g., Paxman et al., 2016, Figure 2d) and Antarctica generally (Hirt, 2014). Paxman et al. (2016) recognized this advantage for the coherence method of T_e estimation on the Antarctic ice. The bedrock topography also has a high, and fairly uniform, variance (Figure S1), mostly $>10^{3.5}$ m^2. This should not cause T_e to be overestimated, according to Kirby and Swain (2009).

In wavelet analysis, there is a trade-off between resolution in the space (x) and wavenumber (k) domains, and a choice must be made to prioritize one at the expense of the other. We use the fan wavelet, formed from a superposition of rotated Morlet wavelets (J. F. Kirby, 2005) whose space/wavenumber domain resolution properties are determined by the value of the Morlet wavelet's central wavenumber, k_0. Approximately, values of $k_0 < 3.5$ prioritize spatial resolution, while setting $k_0 > 7.5$ prioritizes wavenumber resolution; values around 5–6 yield moderate resolution in both domains (Kirby & Swain, 2011). The value we use here, 2.668, gives high spatial resolution but comparatively poor wavenumber resolution. Since T_e is estimated in the wavenumber domain via the Bouguer coherence transition wavelength, one might expect low-k_0 values to yield less accurate elastic thicknesses because the variation of coherence, $\gamma^2(k)$, with wavenumber is less well defined. However, we have found that, while the absolute T_e values are indeed less accurate, the relative T_e differences between proximal spatial locations are well-mapped (Kirby & Swain, 2011). We believe that prioritizing spatial resolution, with the corresponding well-defined relative T_e values, is more important than prioritizing absolute T_e values when mapping tectonic structures. Some examples of synthetic models (Kirby & Swain, 2011) with simple T_e structures illustrate the sizes of features that can be recovered with different k_0 values; for example using $k_0 = 2.668$ it should be possible to recover a linear low-T_e belt of width 200–300 km, though its amplitude may be reduced by 50%–60% relative to reality.

The coherence method normally requires gridded sets of topography and Bouguer gravity anomaly data. Here we use RET data (rock-equivalent topography), with layers of ice and water condensed to rock layers using standard densities. Initially we used the Earth2014 compilation (Hirt & Rexer, 2015), which includes the Bedmap2 data (Fretwell et al., 2013) of surface and sub-ice elevations from Antarctica, but here we use the newer BedMachine data (Morlighem et al., 2020), calculating RET from the three grids supplied: of surface and bedrock elevations and ice thickness. Figure 1 shows the bedrock grid.

We have used two gravity data sets: (1) TIM_R6e (Zingerle et al., 2019) is an extended version of the satellite-only global gravity field model TIM_R6 which includes additional terrestrial data over GOCE's polar gap areas; and (2) a gravity grid compiled from terrestrial data (Scheinert et al., 2016) including airborne and ship surveys. The free air gravity anomalies in the grids were converted to simple Bouguer anomalies using the RET data. All the grids used a 20 × 20 km point spacing, and a polar stereographic projection having a true scale at 71°S latitude (Scheinert et al., 2016).

The satellite gravity model extends to harmonic degree and order 300, equivalent to a wavelength of ~130 km. If this represents the spatial resolution of the gravity model then it should allow the coherence method to resolve T_e values smaller than 10 km (Kirby & Swain, 2008), but in practice this limit is ~15 km

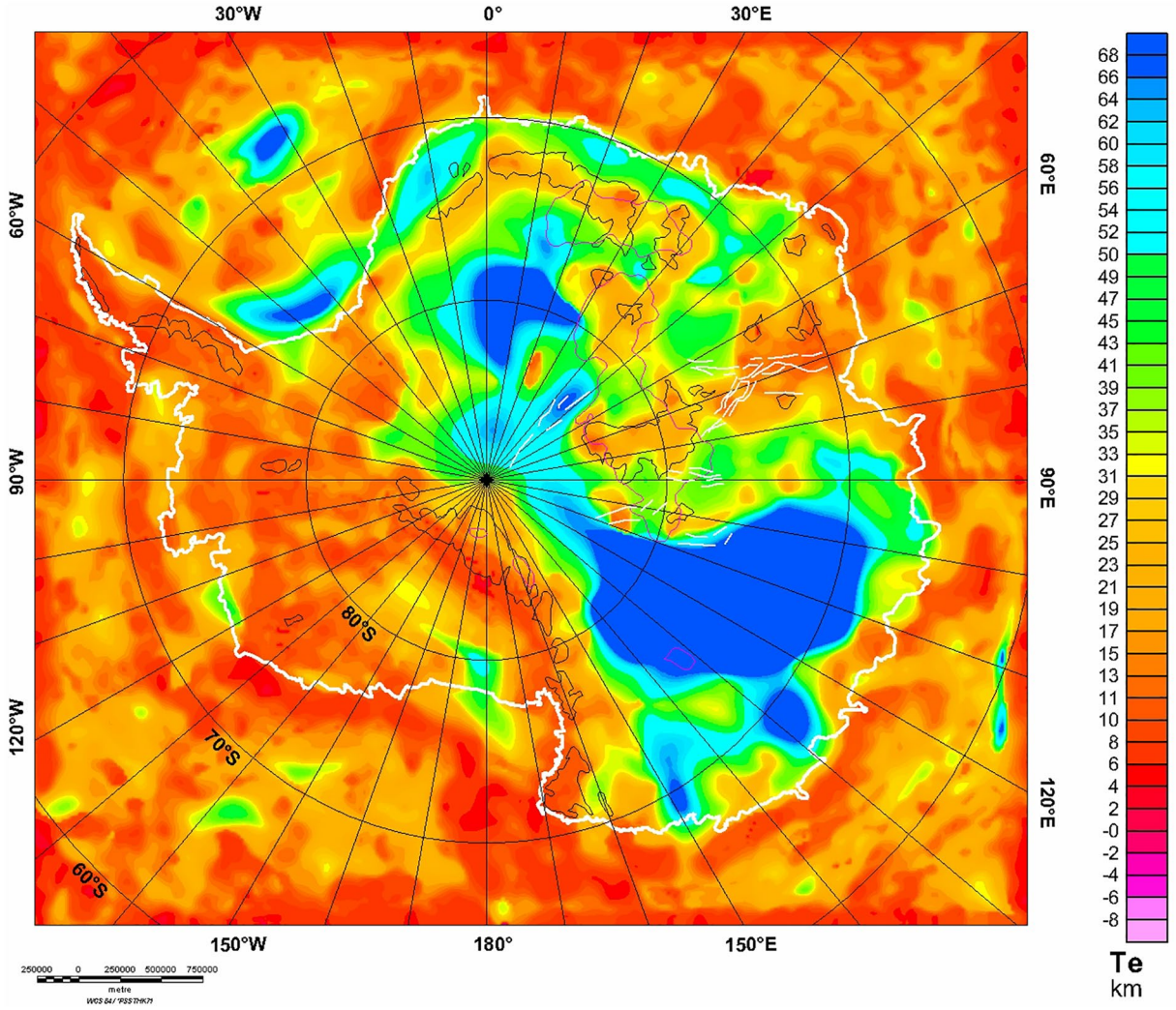

Figure 2. Wavelet T_e using TIM_R6e gravity data (Zingerle et al., 2019) and RET (rock-equivalent topography) from BedMachine data (Morlighem et al., 2020). $k_0 = 2.668$. Red line = 43 km crustal thickness contour. Black line = 1,000 m Bedrock contour. Thin white lines = East Antarctic Rift System.

(McKenzie et al., 2014). The satellite data set is known to be very accurate, but comparing it with the terrestrial free air data (Scheinert et al., 2016) reveals areas of disagreement due to some surveys made in the pre-GPS era that the latter includes. The terrestrial data set has higher spatial resolution and consequently measures lower T_e values. Apart from this difference the T_e maps we have derived from these two data sets are very similar. We present in Figure 2 the result using TIM_R6e. The T_e map made using the terrestrial data is shown for comparison in Figure S6.

Both maps show linear T_e lows with minimum half-amplitude width ~200 km, in agreement with synthetic model tests (Kirby & Swain, 2011). Very similar results were recently presented by Chen et al. (2018) which also used our wavelet-coherence method but gave T_e maps for four different resolutions. Their map made using the same resolution as ours ($k_0 = 2.668$) is very similar to our Figure 2, but their preferred map used a lower resolution than ours ($k_0 = 3.773$) in which some of the narrower features are not present, which is precisely what happens with the synthetic model tests (Kirby & Swain, 2011).

As an additional test of the resolution of our map, we applied our method with $k_0 = 2.668$ to the data for East Africa for comparison with the map of Pérez-Gussinyé et al. (2009) which used a multiple-windowed Slepian multi-taper method, resulting in remarkably high spatial resolution. The tectonic development of the older parts of Africa is also thought to be similar to that of East Antarctica. The resulting T_e map, using

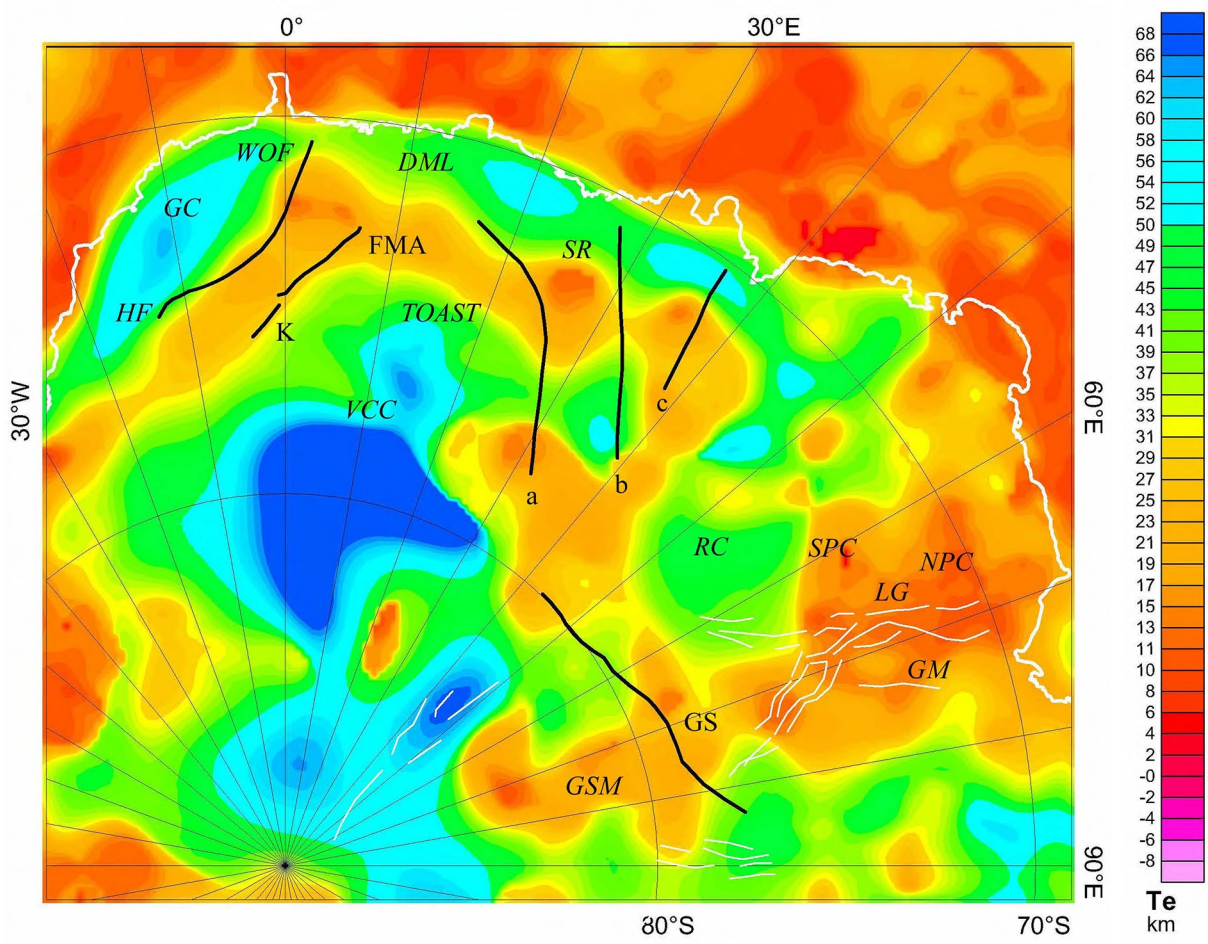

Figure 3. Part of T_e map from Figure 2 with geological features and aeromagnetic lineaments. DML, Dronning Maud Land; GC, Grunehogna craton; GSM, Gamburtsev Subglacial Mountains; GM, Grove Mountains; HF, Heimefront shear zone; NPC, Northern Prince Charles Mountains; LG, Lambert Graben; RC, Ruker Craton; SPC, Southern Prince Charles Mountains; SR, Sør Rondane; WOF, western orogenic front of EAAO (Reidel et al., 2013); K, Kohnen lineament & FMA, Forster magnetic anomaly (Mieth & Jokat, 2014); a, b, c (from Ruppel et al., 2018); GS, Gamburtsev Suture (Ferraccioli et al., 2011); TOAST (Tonian Oceanic Arc Superterrane; Jacobs et al., 2015); VCC, Valkyrie cryptic Craton (Jacobs et al., 2020); thin white lines are the East Antarctic Rift System.

GOCO03s gravity and Earth2014 topography data (Figure S2), shows most of the features in Figure 7 of Pérez-Gussinyé et al. (2009), and moreover the variance of the topography (Figure S3) is similar in range to that of our Figure S1.

4. T_e Results

Our T_e map (Figure 2) shows that much of inland East Antarctica has high T_e, as expected of a craton, separated from the low-T_e Transantarctic Mountains (TAM in Figure 1) by a steep gradient. Both Chen et al. (2018) and Ji et al. (2017) mapped T_e around the TAM and found variations very similar to those in our Figure 2 (they used the same software). Paxman et al. (2019b) used their results in constructing a hypothetical T_e model of the TAM (their Figure 2) showing very low T_e (<10 km) in a narrow strip along the mountain front, simulating a plate break, rising to higher values (~60 km) over the Wilkes Subglacial Basin (WSB) to the west.

Superimposed on the high T_e between 30°W and 80°E is a sinuous line of low T_e connecting the coast-parallel mountains of Dronning Maud Land with the Gamburtsevs and joining the much broader low-T_e zone around the Lambert Graben (LG, Figure 3). This low T_e line follows old orogenic trends and links up with pervasive 500+ Myr basement structures. Figure 2 shows that it correlates with both high bedrock

topography and thicker crust suggesting that these mountains might have been formed with similar tectonic events and at a similar time (An et al., 2015b), though some of the topography could be younger due to reactivation.

Figure 3 is a more detailed image for East Antarctica between 20°W and 90°E showing aeromagnetic lineaments and features referred to in the text. The lineaments were retrieved from the ADMAP-2 data compilation (A. V. Golynsky et al., 2018), after reducing it to the pole (Arkani-Hamed, 1988); in most cases, this yielded unambiguous curvilinear anomalies. In western Dronning Maud Land the Grunehogna Craton (*GC*, Figure 3) forms a distinctive high-T_e zone between the coast and the mountains (Figure 2 and 1,000 m bedrock contour). These mountains lie within the Mesoproterozoic Maud Belt, but at their SW end, the Heimefront (HF) Shear Zone is exposed. This originated within the Maud Belt from the oblique collision between the volcanic arc and the Kaapvaal Craton at ~1,080 Ma (Jacobs et al., 1993; Jacobs & Thomas, 2004). It was reactivated during dextral transpressional tectonics in Ediacaran/Cambrian times that affected the East African Antarctic Orogen (EAAO; Bauer et al., 2016). Aeromagnetic data (Golynsky & Jacobs, 2001) reveal that the HF shear zone separates high amplitude aeromagnetic anomalies over largely unreworked ca 1.2 Ga arc crust similar to the Namaqua-Natal belt (Wang et al., 2020) from a long-wavelength low over the EAAO. Further to the north, high resolution aeromagnetic data show that the orogenic front flanks the slightly younger Maud Belt and controls the location of the Jurassic Jutulstraumen rift (Ferraccioli et al., 2005).

Besides the Grunehogna Craton, there are two other cratons in Dronning Maud Land that show high-T_e zones—the Ruker and Valkyrie Cratons (Figure 3). The Ruker Craton is exposed in the Southern Prince Charles Mountains. Its T_e anomaly is smaller in amplitude than the others, but the version using alternate data sets (Figure S6) is larger. The Valkyrie cryptic craton is not exposed and was identified in the ADMAP-2 aeromagnetic compilation by A. V. Golynsky et al. (2018) and also by Jacobs et al. (2020).

Dronning Maud Land now has relatively good aeromagnetic coverage and a number of key magnetic features have been identified that appear to be associated with the low-T_e zone (Figure 3). The western orogenic front of the EAAO was largely defined from aeromagnetic data (Mieth & Jokat, 2014; Riedel et al., 2013) as were the Forster magnetic anomaly (FMA) and Kohnen lineament (K). The FMA and K lineaments were identified by Riedel et al. (2013) as the eastern front of the EAAO, the latter because of its similarity to the HF anomaly (Golynsky & Jacobs, 2001; Mieth & Jokat, 2014). To its E and S lies a large area of subdued NW-SE striking anomalies (Mieth & Jokat, 2014) extending to >25°E and interpreted from outcrop as a Tonian-age composite oceanic arc superterrane, or TOAST (Jacobs et al., 2015)—see Figure 3. Glacial erratics also support this interpretation and indicate that there was an older Stenian-age precursor. A geological map by Sirevaag et al. (2018, Figure 2) shows the contact between the Maud Belt and the TOAST between 20°W and 15°E. The low-T_e zone coincides with the Maud Belt between these longitudes on this map. Further east lies Sør Rondane, where three magnetic lineaments (a, b, c) have been interpreted (Ruppel et al., 2018) trending S and connecting the E end of the coast-parallel segment of the low-T_e zone to its continuation to the SE. This in turn connects to the low-T_e zone centered on the Gamburtsevs, with another suture (GS) interpreted from aeromagnetic data (Ferraccioli et al., 2011) joining them along 80°S. Both of these low-T_e zones coincide with subglacial mountains.

Our low-T_e corridor (Figure 2) heads north from the Gamburtsevs and broadens into a ~750 km-wide zone centered on the Lambert Graben (Figure 3). It includes the North and South Prince Charles Mountains west of the Lambert Graben, and the Grove Mountains to its east (Figure 3). It correlates quite well with the Lambert Graben and other faults of the East Antarctic Rift system, but the rifts to the Southeast, some of which are seismically active (Lough et al., 2018), show only a generalized correlation with the low-T_e zones, as the T_e map resolution is insufficient to show this in detail.

A T_e value of <15 km has been reported for the Gamburtsevs (Paxman et al., 2016) using free-air admittance as well as Bouguer coherence, which agrees with our Figure 2. Wavelet admittance estimates are noisier than coherence and do not allow high spatial resolution T_e mapping, but we used the method to make T_e estimates from admittances averaged over 500 km square areas over (a) the Gamburtsevs and (b) the high-T_e region of Wilkes land (over the Aurora subglacial basin), obtaining values of 20 km and 100 km, respectively (Figures S4, S5A, and S5B), in reasonable agreement with Figure 2. The graphs also show that the free-air

admittance does not tend to zero at long wavelengths, as also noted by Paxman et al. (2016), which is a possible indicator of mantle convection. We fitted the observed admittances with a model including convection as well as flexure (J. F. Kirby & Swain, 2014) as can be seen in Figures S5A and S5B.

As Eagles et al. (2018) note, the coast-parallel mountains of central DML form one of the world's great escarpments, which evolved from the extended continental margin resulting from the breakup of Gondwana in Jurassic times. It has a relief of >5 km, with peaks up to 3,200 m above sea level, and is ~200 km inland from the present margin. Sirevaag et al. (2018) used apatite fission track (APT), and other thermochronological methods to study the post-Pan-African tectonic evolution of central DML. Their results are consistent with the formation and evolution of Permian to Jurassic basins followed by flexural uplift of the passive margin both heralding and following the break-up of Gondwana. Eagles et al. (2018) showed that there was also clearly activity linked to passive margin development and erosion that occurred inland of the mountains.

Figures 2 and 3 show a convincing correlation between the low-*Te* corridor and both the mountains (including subglacial ones) and their roots, and also structures inferred from aeromagnetic surveys, some of which have been proposed to result from Pan-African age sutures e.g. the Forster magnetic anomaly (Riedel et al., 2013) and the Gamburtsev Suture (Ferraccioli et al., 2011). However, the present-day mountains are unlikely to be that old (e.g., Paxman et al., 2016) so the Sirevaag et al. (2018) and Eagles et al. (2018) scenarios seem preferable.

5. The Gamburtsev Subglacial Mountains

The Gamburtsevs are encompassed by a network of rifts and Ferraccioli et al. (2011), proposed that these rifts are similar in origin to the East African Rifts in forming around the Ruker Craton and Gamburtsev Province just as the East African Rifts developed around the Tanzania Craton. However, the latter has a high T_e (>60 km; Pérez-Gussinyé et al., 2009) whereas the T_e of the Gamburtsevs is <15 km, so the analogy in imperfect.

In the Ferraccioli et al. (2011) model, four interconnecting processes contribute to the uplift of the mountains: root buoyancy, denudation, mechanical unloading and valley incision. In the models of Paxman et al. (2016), T_e does not have a major influence on the magnitude of flexural uplift. They also found that only 17%–25% of total GSM elevation is attributable to valley incision, so ~80% must result from tectonic or dynamic mechanisms.

Shen et al. (2018) suggested eclogitization as a possible cause of the low shear velocity zone that they discovered in the uppermost ~50 km of the mantle beneath the Gamburtsevs (see Section 2). This is an attractive idea since, besides having low shear velocity, eclogite can be both dense and very weak (Austrheim, 1991). Thus they could contribute to the apparently high densities in the lowest crustal layer of the gravity models of Ferraccioli et al. (2011), while a weak layer just below the crust could cause decoupling between crust and mantle and hence lower the T_e of the lithosphere (see Section 2). Eclogite are unusual rocks that result from high-pressure metamorphism of either oceanic crust in subduction zones or continental crust (e.g., granulitic) in orogenic collision zones. It is thought that fluids are necessary for complete eclogitization, or its reversal before eclogite are exhumed. According to Richardson and England (1979), the high-density phase of eclogite can persist for tens of millions of years giving anomalously low surface elevation of the thickened continent and inhibiting erosion.

6. Conclusions

Three main low-T_e zones are revealed in East Antarctica by our new study:

1. The Permian to Cretaceous age Lambert Rift and the eastern branch of the East Antarctic Rift System.
2. An arcuate coast-parallel region of low T_e occurs in western Dronning Maud Land over the Maud Belt and in central Dronning Maud Land. These are Grenvillian-age lithospheric domains that were pervasively reworked by the Pan-African age (~600–500 Ma) East Antarctic Orogen. The region was also the site of younger Mesozoic to Cenozoic uplift related to the formation and subsequent evolution of the Dronning Maud Land passive margin escarpment (Eagles et al., 2018; Sirevaag et al., 2018).

3. A linear belt of low T_e stretches from the GSM to parts of the Tonian Oceanic Arc Superterrane (Ruppel et al., 2018). Our analysis, using the wavelet version of Forsyth's (1985) method, which inverts the data for lower crustal loads in the process of estimating T_e, indicates that a low-T_e scenario is more likely for the GSM, in agreement with the results of Paxman et al. (2016). We infer that upper mantle eclogitization processes proposed from independent seismic shear velocity models (Shen et al., 2018) occurred during Pan-African age orogenic events and contributed to weakening of the older Precambrian lithosphere. However, the anomalously high elevation of the entire sector of East Antarctica from ~100°E to DML is likely due to a combination of thick crust and lithosphere and dynamic topography effects (e.g., Pappa et al., 2019b) linked to upper mantle convection, which is supported by the fact that free-air admittance over much of East Antarctica does not tend to zero at long wavelengths.

Data Availability Statement

The T_e data displayed in Figure 2 are archived in the PANGAEA data repository in the form of a Geosoft grid file with an ASCII equivalent (Swain & Kirby, 2020).

Acknowledgments
The authors thank the two anonymous referees for their comments which helped considerably in revising the original paper. The authors thank Ian Fitzsimons for assistance with Antarctic geology and encouraging the early development of this paper. The authors thank Tom Jordan of the British Antarctic Survey for supplying the locations of the East Antarctic Rift System.

References

Aitken, A. R. A., Young, D. A., Ferraccioli, F., Betts, P. G., Greenbaum, J. S., Richter, T. G., et al. (2014). The subglacial geology of Wilkes Land, East Antarctica. *Geophysical Research Letters*, *41*, 2390–2400. https://doi.org/10.1002/2014GL059405

An, M.-J., Wiens, D. A., Zhao, Y., Feng, M., Nyblade, A., Kanao, M., et al. (2015a). Temperature, lithosphere-asthenosphere boundary, and heat flux beneath the Antarctic Plate inferred from seismic velocities. *Journal of Geophysical Research: Solid Earth*, *120*, 8720–8742. https://doi.org/10.1002/2015JB011917

An, M.-J., Wiens, D. A., Zhao, Y., Feng, M., Nyblade, A. A., Kanao, M., et al. (2015b). S-velocity model and inferred Moho topography beneath the Antarctic Plate from Rayleigh waves. *Journal of Geophysical Research: Solid Earth*, *120*, 359–383. https://doi.org/10.1002/2014JB011332

Arkani-Hamed, J. (1988). Differential reduction-to-the-pole of regional magnetic anomalies. *Geophysics*, *53*, 1592–1600.

Audet, P., & Burgmann, R. (2011). Dominant role of tectonic inheritance in supercontinent cycles. *Nature Geoscience*, *4*, 184–187.

Austrheim, H. (1991). Eclogite formation and dynamics of crustal roots under continental collision zones. *Terra Nova*, *3*, 492–499.

Bauer, W., Siemes, H., Speath, G., & Jacobs, J. (2016). Transpression and tectonic exhumation in the Heimefrontfjella, western orogenic front of the East African/Antarctic Orogen, revealed by quartz textures of high strain domains. *Polar Research*, *35*, 25420. http://dx.doi.org/10.3402/polar.v35.25420

Boger, S. D. (2011). Antarctica–before and after Gondwana. *Gondwana Research*, *19*, 335–371.

Burov, E. B., & Diament, M. (1995). The effective elastic thickness (T_e) of continental lithosphere: What does it really mean?. *Journal of Geophysical Research*, *100*, 3905–3927.

Chen, B., Haeger, C., Kaban, M. K., & Petrunin, A. G. (2018). Variations of the effective elastic thickness reveal tectonic fragmentation of the Antarctic lithosphere. *Tectonophysics*, *746*, 412–424.

Cianfarra, P., & Maggi, M. (2017). Cenozoic extension along the reactivated Aurora Fault Systemic the East Antarctic Craton. *Tectonophysics*, *703–4*, 135–143.

Cianfarra, P., & Salvini, F. (2016). Origin of the Adventure Subglacial Trench linked to Cenozoic extension in the East Antarctic Craton. *Tectonophysics*, *670*, 30–37.

Cox, S. E., Thomson, S. N., Reiners, P. W., Hemming, S. R., & Van De Flierdt, T. (2010). Extremely low long-term erosion rates around the Gambertsev Mountains in interior East Antarctica. *Geophysical Research Letters*, *37*, L22307. https://doi.org/10.1029/2010GL045106

Creyts, T. T., Ferraccioli, F., Bell, R. E., Wolovick, M., Corr, H., Rose, K. C., et al. (2014). Freezing of ridges and water networks preserves the Gamburtsev Subglacial Mountains for millions of years. *Geophysical Research Letters*, *41*, 8114–8122. https://doi.org/10.1002/2014GL061491

Eagles, G., Karlsson, N. B., Ruppel, A., Steinhage, D., Jokat, W., & Läufer, A. (2018). Erosion at extended continental margins: Insights from new aerogeophysical data in eastern Dronning Maud Land. *Gondwana Research*, *63*, 105–116.

Ferraccioli, F., Finn, C. A., Jordan, T. A., Bell, R. E., Anderson, L. M., & Damaske, D. (2011). East Antarctic rifting triggers uplift of the Gamburtsev Mountains. *Nature*, *479*, 388–392.

Ferraccioli, F., Jones, P., Curtis, M. L., Leat, P. T., & Riley, T. R. (2005). Tectonic and magmatic patterns in the Jutulstraumen rift region, East Antarctica, as imaged from high resolution aeromagnetic data. *Earth Planets and Space*, *57*, 767–780.

Fisher, K. M. (2002). Waning buoyancy in the crustal roots of old mountains. *Nature*, *417*, 933–936.

Fitzsimons, I. C. W. (2000). Grenville-age basement provinces in East Antarctica: Evidence for three separate collisional orogens. *Geology*, *28*, 879–882.

Fitzsimons, I. C. W. (2003). Proterozoic basement provinces of southern and southwestern Australia, and their correlation with Antarctica. *Geological Society London Special Publications*, *206*, 93–130.

Forsyth, D. W. (1985), Subsurface loading and estimates of the flexural rigidity of continental lithosphere, *Journal of Geophysical Research*, *90*, 12623–12632. https://doi.org/10.1029/JB090iB14p12623

Fretwell, P., Pritchard, H. D., Vaughan, D. G., Bamber, J. L., Barrand, N. E., Bell, R., et al. (2013). Bedmap2: Improved ice bed, surface and thickness datasets for Antarctica. *The Cryosphere*, *7*, 375–393.

Golynsky, A. V., Ferraccioli, F., Hong, J. K., Golynsky, D. A., von Frese, R. R. B., Young, D. A., et al. (2018). New magnetic anomaly map of the Antarctic. *Geophysical Research Letters*, *45*, 6437–6449. https://doi.org/10.1029/2018GL078153

Golynsky, A., & Jacobs, J. (2001). Grenville-age versus Pan-African magnetic anomaly imprints in Western Dronning Maud Land, East Antarctica. *The Journal of Geology*, *109*, 136–142.

Harley, S. L., Fitzsimons, I. C. W., & Zhao, Y. (2013). Antarctica and supercontinent evolution: historical perspectives, recent advances and unresolved issues. *Geological Society London Special Publications*, *383*, 1–34.

Hirt, C. (2014). GOCE's view below the ice of Antarctica: Satellite gravimetry confirms improvements in Bedmap2 bedrock knowledge. *Geophysical Research Letters*, *41*, 5021–5028. https://doi.org/10.1029/2018GL078153

Hirt, C., & Rexer, M. (2015). Earth2014: 1 arc-min shape, topography, bedrock and ice-sheet models—available as gridded data and degree—10,800 spherical harmonics. *International Journal of Applied Earth Observation and Geoinformation*, *39*, 103–112. https://doi.org/10.1016/j.jag.2015.03.001

Jacobs, J., Elburg, M., Läufer, A., Kleinhanns, I. C., Henjes-Kunst, F., Estrada, S., et al. (2015). Two distinct Late Mesoproterozoic/Early Neoproterozoic basement provinces in central/eastern Dronning Maud Land, East Antarctica: The missing link, 15–21°E. *Precambrian Research*, *265*, 249–272.

Jacobs, J., Mikhalsky, E., Henjes-Kunst, F., Läufer, A., Thomas, R. J., Elburg, M. A., et al. (2020). Neoproterozoic geodynamic evolution of easternmost Kalahari: Constraints from U-Pb-Hf-O zircon, Sm-Nd isotope and geochemical data from the Schirmacher Oasis, East Antarctica. *Precambrian Research*, *342*, 105553.

Jacobs, J., & Thomas, R. J. (2004). Himalayan-type indenter-escape tectonics model for the southern part of the late Neoproterozoic-early Paleozoic East African-Antarctic orogen. *Geology*, *32*, 721–724.

Jacobs, J., Thomas, R. J., & Weber, K. (1993). Accretion and indentation tectonics at the southern edge of the Kaapvaal craton during the Kibaran (Grenville) orogeny. *Geology*, *21*, 203–206.

Ji, F., Gao, J., Shen, Z., Zhang, Q., & Li, Y. (2017). Variations of the effective elastic thickness over the Ross Sea and Transantarctic Mountains and implications for their structure and tectonics. *Tectonophysics*, *717*, 127–138. https://doi.org/10.1016/j.tecto.2017.07.011

Kirby, J. F. (2005). Which wavelet best reproduces the Fourier power spectrum? *Computers & Geosciences*, *31*(7), 846–864. https://doi.org/10.1016/j.cageo.2005.01.014

Kirby, J. F. (2014). Estimation of the effective elastic thickness of the lithosphere using inverse spectral methods: The state of the art. *Tectonophysics*, *631*, 87–116.

Kirby, J. F., & Swain, C. J. (2008). An accuracy assessment of the fan wavelet coherence method for elastic thickness estimation. *Geochemistry, Geophysics, Geosystems*, *9*, Q03022. https://doi.org/10.1029/2007GC001773

Kirby, J. F., & Swain, C. J. (2009). A reassessment of spectral T_e estimation in continental interiors: The case of North America. *Journal of Geophysical Research*, *114*, B08401. https://doi.org/10.1029/2009JB006356

Kirby, J. F., & Swain, C. J. (2011). Improving the spatial resolution of effective elastic thickness estimation with the fan wavelet transform. *Computers & Geosciences*, *37*, 1345–1354.

Kirby, J. F., & Swain, C. J. (2014). The long-wavelength admittance and effective elastic thickness of the Canadian Shield. *Journal of Geophysical Research: Solid Earth*, *119*, 5187–5214. https://doi.org/10.1002/2013JB010578

Lough, A. C., Wiens, D. A., & Nyblade, A. (2018). Reactivation of ancient Antarctic rift zones by intraplate seismicity. *Nature Geoscience*, *11*(7), 515–519. https://doi.org/10.1038/s41561-018-0140-6

Lowry, A. R., & Smith, R. B. (1995). Strength and rheology of the western U.S. Cordillera. *Journal of Geophysical Research*, *100*(17947–17), 963.

Maritati, A., Danišík, M., Halpin, J. A., Whittaker, J. M., & Aitken, A. R. (2020). Pangea rifting shaped the East Antarctic landscape. *Tectonics*, *39*, e2020TC006180. https://doi.org/10.1029/2020TC006180

McKenzie, D. (2003). Estimating T_e in the presence of internal loads. *Journal of Geophysical Research*, *108*, 2438. https://doi.org/10.1029/2002JB001766

McKenzie, D., Yi, W., & Rummel, R. (2014). Estimates of T_e from GOCE data. *Earth and Planetary Science Letters*, *399*, 116–127.

Mieth, M., & Jokat, W. (2014). New aeromagnetic view of the geological fabric of southern Dronning Maud Land and Coats Land, East Antarctica. *Gondwana Research*, *25*, 358–267.

Morlighem, M., Rignot, E., Binder, T., Blankenship, D., Drews, R., Eagles, G., et al (2020). Deep glacial troughs and stabilizing ridges unveiled beneath the margins of the Antarctic ice sheet. *Nature Geoscience*, *13*, 132–137.

Morrissey, L. J., Hand, M., & Kelsey, D. E. (2015). Multi-stage metamorphism in the Rayner–Eastern Ghats Terrane: P–T–t constraints from the northern Prince Charles Mountains, east Antarctica. *Precambrian Research*, *267*, 137–163.

O'Donnell, J. P., & Nyblade, A. A. (2014). Antarctica's hypsometry and crustal thickness: Implications for the origin of anomalous topography in East Antarctica. *Earth and Planetary Science Letters*, *388*, 143–155.

Pappa, F., Ebbing, J., & Ferraccioli, F. (2019a). Moho depths of Antarctica: Comparison of seismic, gravity, and isostatic results. *Geochemistry, Geophysics, Geosystems*, *20*, 1629–1645. https://doi.org/10.1029/2018GC008111

Pappa, F., Ebbing, J., Ferraccioli, F., & van der Wal, W. (2019b). Modeling satellite gravity gradient data to derive density, temperature, and viscosity structure of the Antarctic lithosphere. *Journal of Geophysical Research: Solid Earth*, *124*, 12053–12076. https://doi.org/10.1029/2019JB017997

Paxman, G. J. G., Jamieson, S. S., Hochmuth, K., Gohl, K., Bentley, M. J., Leitchenkov, G., & Ferraccioli, F. (2019a). Reconstructions of Antarctic topography since the Eocene–Oligocene boundary. *Palaeogeography, Palaeoclimatology, Palaeoecology*, *535*, 109346.

Paxman, G. J. G., Jamieson, S. S. R., Ferraccioli, F., Bentley, M. J., Ross, N., Watts, A. B., et al. (2019b). The role of lithospheric flexure in the landscape evolution of the Wilkes Subglacial Basin and Transantarctic Mountains, East Antarctica. *Journal of Geophysical Research: Earth Surface*, *124*, 812–829. https://doi.org/10.1029/2018JF004705

Paxman, G. J. G., Watts, A. B., Ferraccioli, F., Jordan, T. A., Bell, R. E., Jamieson, S. S. R., & Finn, C. A. (2016). Erosion-driven uplift in the Gamburtsev Subglacial mountains of East Antarctica. *Earth and Planetary Science Letters*, *452*, 1–14.

Pérez-Gussinyé, M., Metois, M., Fernández, M., Vergés, J., Fullea, J., & Lowry, A. R. (2009). Effective elastic thickness of Africa and its relationship to other proxies for lithospheric structure and tectonics. *Earth and Planetary Science Letters*, *287*, 152–167.

Richardson, S. W., & England, P. C. (1979). Metamorphic consequences of crustal eclogite production in overthrust orogenic zones. *Earth and Planetary Science Letters*, *42*, 183–190.

Riedel, S., Jacobs, J., & Jokat, W. (2013). Interpretation of new regional aeromagnetic data over Dronning Maud land (East Antarctica). *Tectonophysics*, *585*, 161–171.

Ritzwoller, M. H., Shapiro, N. M., Levshin, A. L. & Leahy, G. M. (2001), Crustal and upper mantle structure beneath Antarctica and surrounding oceans. *Journal of Geophysical Research*, *106*, 30645–30670.

Rose, K. C., Ferraccioli, F., Jamieson, S. S. R., Bell, R. E., Corr, H., Creyts, T. T., et al. (2013). Early East Antarctic ice sheet growth recorded in the landscape of the Gamburtsev Subglacial Mountains. *Earth and Planetary Science Letters*, *375*, 1–12.

Ruppel, A., Jacobs, J., Eagles, G., Läufer, A., & Jokat, W. (2018). New geophysical data from a key region in East Antarctica: Estimates for the spatial extent of the Tonian Oceanic Arc Super Terrane (TOAST). *Gondwana Research*, *59*, 97–107.

Scheinert, M., Ferraccioli, F., Schwabe, J., Bell, R., Studinger, M., Damaske, D., et al. (2016). New Antarctic gravity anomaly grid for enhanced geodetic and geophysical studies in Antarctica. *Geophysical Research Letters*, *43*, 600–610. https://doi.org/10.1002/2015GL067439

Shen, W., Wiens, D. A., Anandakrishnan, S., Aster, R. C., Gerstoft, P., Bromirski, P. D., et al (2018). The crust and upper mantle structure of Central and West Antarctica from Bayesian inversion of Rayleigh wave and receiver functions. *Journal of Geophysical Research: Solid Earth*, *123*, 7824–2849. https://doi.org/10.1029/2017JB015346

Sirevaag, H., Ksienzyk, A. K., JacobsDunkl, J. I., & Läufer, A. (2018). Tectono-thermal evolution and morphodynamics of the central Dronning Maud Land, East Antarctica, based on new thermochronological data. *Geosciences*, *8*(11), 390. https://doi.org/10.3390/geosciences8110390

Swain, C. J., & Kirby, J. (2020). Effective Elastic Thickness (T_e) Map of Antarctica from wavelet coherence of gravity and rock-equivalent topography. *PANGAEA*, *90*(9), 883–902. https://doi.org/10.1594/PANGAEA.919450

Tassara, A., Swain, C., Hackney, R., & Kirby, J. (2007). Elastic thickness structure of South America estimated using wavelets and satellite-derived gravity data. *Earth and Planetary Science Letters*, *253*, 17–36.

Thomson, S. N., Reiners, P. W., Hemming, S. R., & Gehrels, G. E. (2013). The contribution of glacial erosion to shaping the hidden landscape of East Antarctica. *Nature Geoscience*, *6*, 203–207.

van de Flierdt, T., Gehrels, G. E., Goldstein, S. L., & Hemming, S. R. (2007). Pan-African age of the Gamburtsev mountains? In A. K. Cooper, et al. (Eds.), *Antarctica: A Keystone in a changing world—online proceedings of the 10th ISAES X*. (p. 4)., USGS Open-File Report.

van de Flierdt, T., Hemming, S. R., Goldstein, S. L., Gehrels, G. E., & Cox, S. E. (2008). Evidence against a young volcanic origin of the Gamburtsev Subglacial Mountains, Antarctica. *Geophysical Research Letters*, *35*, L21303. https://doi.org/10.1029/2008GL035564

Veevers, J. J., & Saeed, A. (2008). Gamburtsev Subglacial Mountains provenance of Permian–Triassic sandstones in the Prince Charles Mountains and offshore Prydz Bay: Integrated U–Pb and TDM ages and host-rock affinity from detrital zircons. *Gondwana Research*, *14*, 316–342.

Veevers, J. J., & Saeed, A. (2011). Age and composition of Antarctic bedrock reflected by detrital zircons, erratics, and recycled microfossils in the Prydz Bay-Wilkes Land-Ross Sea-Marie Byrd Land sector (70°–240°E). *Gondwana Research*, *20*, 710–738.

Veevers, J. J., & Saeed, A. (2013). Age and composition of Antarctic sub-glacial bedrock reflected by detrital zircons, erratics, and recycled microfossils in the Ellsworth Land-Antarctic Peninsula-Weddell Sea-Dronning Maud Land sector (240°E-0°-015°E). *Gondwana Research*, *23*, 296–332.

Wang, C.-C., Jacobs, J., Elburg, M. A., Läufer, A., Thomas, R. J., & Elvevold, S. (2020). Grenville-age continental arc magmatism and crustal evolution in central Dronning Maud Land (East Antarctica): Zircon geochronology and Hf-O isotopic evidence. *Gondwana Research*, *82*, 108–127.

Zachos, J. C., Pagani, M., Sloan, L., Thomas, E., & Billups, K. (2001). Trends, rhythms, and aberrations in global climate 65 Ma to present. *Science*, *292*, 686–693.

Zingerle, P., Brockmann, J. M., Pail, R., Gruber, T., & Willberg, M. (2019). *The polar extended gravity field model TIM_R6e*. GFZ Data Services. http://doi.org/10.5880/ICGEM.2019.005